Induced pluripotent stem cells derived from rabbits exhibit some characteristics of naïve pluripotency

Pierre Osteil[1,2,3,4,*], Yann Tapponnier[1,2,3,*], Suzy Markossian[1,2,3,4,*], Murielle Godet[1,2,3,4], Barbara Schmaltz-Panneau[5], Luc Jouneau[5], Cédric Cabau[6], Thierry Joly[3,7,8], Thierry Blachère[1,2,3], Elen Gócza[9], Agnieszka Bernat[1,2,3,‡], Martine Yerle[10], Hervé Acloque[10], Sullivan Hidot[1,2,3], Zsuzsanna Bosze[9], Véronique Duranthon[5], Pierre Savatier[1,2,3,4,§] and Marielle Afanassieff[1,2,3,4,§]

[1]INSERM, U846, Stem Cell and Brain Institute, 18 Avenue du Doyen Jean Lépine, F-69500 Bron, France
[2]Stem Cell and Brain Institute, F-69500 Bron, France
[3]Université de Lyon, F-69100 Villeurbanne, France
[4]INRA, USC1361, F-69500 Bron, France
[5]INRA, Biology of Development and Reproduction, F-78352 Jouy-en-Josas, France
[6]INRA, SIGENAE, UR83 Recherches Avicoles, F-37380 Nouzilly, France
[7]ISARA-Lyon, F-69007 Lyon, France
[8]VetAgroSup, UPSP ICE, F-69280 Marcy l'Etoile, France
[9]Institute of Animal Biotechnology, Agricultural Biotechnology Center, H-2100 Godollo, Hungary
[10]INRA, UMR444, F-31326 Castanet Tolosan, France

*These authors contributed equally to this work
‡Present address: Laboratory of Molecular Diagnostics, Intercollegiate Faculty of Biotechnology, Medical University of Gdansk, Poland
§Authors for correspondence (marielle.afanassieff@inserm.fr; pierre.savatier@inserm.fr)

Summary

Not much is known about the molecular and functional features of pluripotent stem cells (PSCs) in rabbits. To address this, we derived and characterized 2 types of rabbit PSCs from the same breed of New Zealand White rabbits: 4 lines of embryonic stem cells (rbESCs), and 3 lines of induced PSCs (rbiPSCs) that were obtained by reprogramming adult skin fibroblasts. All cell lines required fibroblast growth factor 2 for their growth and proliferation. All rbESC lines showed molecular and functional properties typically associated with primed pluripotency. The cell cycle of rbESCs had a prolonged G1 phase and a DNA damage checkpoint before entry into the S phase, which are the 2 features typically associated with the somatic cell cycle. In contrast, the rbiPSC lines exhibited some characteristics of naïve pluripotency, including resistance to single-cell dissociation by trypsin, robust activity of the distal enhancer of the mouse *Oct4* gene, and expression of naïve pluripotency-specific genes, as defined in rodents. According to gene expression profiles, rbiPSCs were closer to the rabbit inner cell mass (ICM) than rbESCs. Furthermore, rbiPSCs were capable of colonizing the ICM after aggregation with morulas. Therefore, we propose that rbiPSCs self-renew in an intermediate state between naïve and primed pluripotency, which represents a key step toward the generation of *bona fide* naïve PSC lines in rabbits.

Introduction

Pluripotent stem cells (PSCs) can exist in two morphologically, molecularly and functionally distinct pluripotent states, designated as the naïve and primed states (Nichols and Smith, 2009). The first rabbit pluripotent stem cell (PSC) lines were produced from New Zealand White rabbit blastocysts in the form of embryonic stem cells [rabbit ESCs (rbESCs)] (Fang et al., 2006; Wang et al., 2007). In their undifferentiated state, rbESCs required both fibroblast growth factor 2 (FGF2) and growth factors of the transforming growth factor (TGF) β family (activin, nodal) for self-renewal (Wang et al., 2008). These results were confirmed in another study, which showed that activin/nodal signaling through Smad2/3 activation was necessary for maintaining the pluripotent status of rbESCs (Honda et al.,

2009). These rbESCs did not colonize rabbit embryos after being injected into blastocysts (Honda et al., 2008). Honda et al. also established rabbit induced PSC lines [rabbit iPSCs (rbiPSCs)] from adult liver and stomach cells (Honda et al., 2010). Similar to rbESCs, rbiPSCs are dependent on FGF2 for self-renewal. Therefore, rbESCs and rbiPSCs seemed to exhibit the cardinal feature of primed pluripotency. However, this conclusion should be moderated because none of these studies evaluated these cell lines for other criteria that demarcate naïve and primed pluripotency; moreover, these studies did not compared these cell lines with rabbit inner cell mass (ICM) cells and PSCs from other species. Therefore, the status of rbESCs and rbiPSCs is yet to be thoroughly evaluated. In our study, we compared rbESCs and rbiPSCs at both molecular and functional levels and

concluded that (*i*) rbESCs do not exhibit all the characteristic features of pluripotency and (*ii*) rbiPSCs exhibit some characteristic features of naïve pluripotency.

Results

Derivation of FGF2-dependent rbESC lines

Twenty-four ICMs isolated from 52 blastocysts by immunosurgery were plated on feeder cells in rbESC medium supplemented with FGF2. Twelve of these ICMs could form outgrowths, of which 4 produced a population of highly proliferating cells that could be routinely passaged more than 40 times. These rbESC lines – designated rbES-4, rbES-8, rbES-18 and rbES-19 – formed flattened colonies of compact cells (Fig. 1A; supplementary material Fig. S1A). They were passaged every 3 days after collagenase II treatment of the colonies, followed by gentle dissociation into small clumps. All attempts to passage these cell lines after trypsinization into single-cell suspensions resulted in extensive differentiation and apoptosis (data not shown). All the 4 lines were positive for alkaline phosphatase activity (Fig. 1B; supplementary material Fig. S1A) and were strictly dependent on FGF2 for self-renewal, as determined by their altered morphology after FGF2 withdrawal for 24 h (Fig. 1C). Conventional Giemsa staining showed a normal chromosome number in all the selected lines (>50 metaphase spreads analyzed: 42XY) (Fig. 1D; supplementary material Fig. S1A). For rbES-18 line, the cells were karyotyped using G-banding, and normal chromosome complements were observed in the 4 analyzed metaphase spreads (Fig. 1E). Immunolabeling showed that all the 4 lines expressed *Oct4* in virtually every cell in the respective populations (Fig. 1F; supplementary material Fig. S3). All the 4 cell lines could undergo *in vitro* differentiation into embryoid bodies (EBs) (Fig. 1H). Differentiation was accompanied by the rapid loss of *Nanog* and *Oct4* expression and upregulation of the ectodermal marker *Nestin* and endodermal marker *Hnf3β*. The mesodermal marker *Flk1* was expressed at robust levels in undifferentiated cells (Fig. 1G). All the 4 rbESC lines could induce teratomas after being injected under the kidney capsules in SCID mice. All teratomas contained derivatives of the 3 embryonic germ layers (Fig. 1I,J; supplementary material Fig. S2A). Therefore, these 4 rbESC lines appeared to exhibit the characteristics of PSCs.

Generation of iPSC lines from adult rabbit fibroblasts

Adult rabbit fibroblasts (rbF) were infected twice at a 48-h interval with a mixture of 4 retroviral vectors that expressed human Oct4, Sox2, Klf4 and c-Myc transcription factors. Three days after the second infection, the rbFs were dissociated and replated on feeder cells in an rbESC medium supplemented with 10 ng/ml FGF2. The culture medium was changed every day thereafter until some colonies with compact morphologies appeared (Fig. 2A). One hundred and eleven clones were selected between the 15th and 29th day after fibroblast infection. These 111 clones were passaged by trypsin dissociation into single-cell suspensions. Twelve clones expressing alkaline phosphatase and capable of rapid proliferation were selected for further studies. At passage 6, 4 of these clones expressed rabbit *Nanog* and *Oct4* at the same level as that in rbESCs (Fig. 2B). For 3 clones – designated rbiPS-B19, rbiPS-B24 and rbiPS-B29 – silencing of all the 4 transgenes was achieved at passage 25 (Fig. 2C). Line rbiPS-B25 did not show suppressed *hc-MYC* transgene expression even after 25 passages and was excluded from all subsequent analysis. Withdrawal of FGF2 induced dramatic morphological changes within 48 h, suggesting

differentiation (Fig. 2D). A normal chromosome number was observed in 2 lines – rbiPS-B19 and rbiPS-B29 (Fig. 2E; supplementary material Fig. S1B). For the rbiPS-B19 cell line, cells were karyotyped using G-banding, and normal chromosome complements were observed in the 20 analyzed metaphase spreads (Fig. 2F). The rbiPS-B24 cell line showed an abnormal 43XX karyotype. Immunolabelling showed that all the 3 cell lines expressed *Oct4* in virtually every cell in the respective populations (Fig. 2G; supplementary material Fig. S3). Differentiation induced by suspension culture resulted in the rapid loss of *Oct4* and *Nanog* expression (Fig. 2H). *HNF3β*, *Flk1* and *Nestin* were already expressed at robust levels in undifferentiated rbiPS-B19 cells. All the 3 lines induced teratomas containing cells that had differentiated into the 3 germ layers after being injected into SCID mice (Fig. 2I; supplementary material Fig. S2B). Most importantly, all iPSC lines could be routinely passaged every 2 days by trypsin dissociation into single-cell suspensions.

Contrasting expression patterns of stage-specific embryonic antigen (SSEAs) and cadherins

The patterns of stage-specific embryonic antigen (SSEA) expression differed between cell types, and all showed considerable heterogeneity. All the 3 rbiPSC lines showed heterogeneous expression of SSEA1, SSEA4, and TRA-1-60, whereas all the 4 rbESC lines expressed only SSEA1 (supplementary material Fig. S3). Distribution of SSEA1 and SSEA4 expression in various cell populations was quantified using flow cytometry (Fig. 3A). SSEA1 was expressed in 30–60% rbESCs and rbiPSCs, compared with 94% mESCs (Fig. 3B). SSEA4 was expressed in 10–40% rbiPSCs and the pattern was complex with these lines, which comprised 4 cell subpopulations: SSEA1$^+$ (32–49%), SSEA4$^+$ (5–12%), double-positive (7–26%), and double-negative (29–37%) cells (Fig. 3C). The distributions between these 4 sub-populations differed between lines and were constant over time in culture (data not shown). We determined whether these 4 populations represented 4 distinct cell types or whether they were capable of converting into each other in culture. To address this each subpopulation was sorted by FACS and subsequently cultured for 1 week (secondary cultures) before analysis by flow cytometry. The heterogeneity originally observed in the unsorted cell population was restored from each subpopulation (Fig. 3C). These results indicate that rbiPSCs existed in 4 interchangeable states (SSEA1$^+$/SSEA4$^+$, SSEA1$^-$/SSEA4$^+$, SSEA1$^+$/SSEA4$^-$, and SSEA1$^-$/SSEA4$^-$), and that the distribution of the 4 populations was cell line specific.

E-cadherin expression is observed in all PSCs regardless of species, whereas N-cadherin is expressed only in mouse Epiblast Stem Cells (EpiSCs) (Tesar et al., 2007). rbESC and rbiPSC lines had different patterns of E- and N-cadherin expression. Immunolabeling showed that all rbESC lines expressed both E- and N-cadherins similar to rhesus ESCs. In contrast, rbiPSC lines expressed only E-cadherin similar to mouse ESCs (Fig. 3D). Each SSEA subpopulation was sorted by FACS, and the expression of E- and N-cadherins was analyzed by qPCR. All subpopulations of rbiPSCs expressed *Cdh1* (E-cadherin) at levels 10- to 100-fold higher than those measured in rbESCs. In contrast, the same subpopulations expressed *Cdh2* (N-cadherin) at levels 10- to 100-fold lower than those measured in rbESCs (Fig. 3E). Therefore, differential expression of E- and N-cadherins was associated with
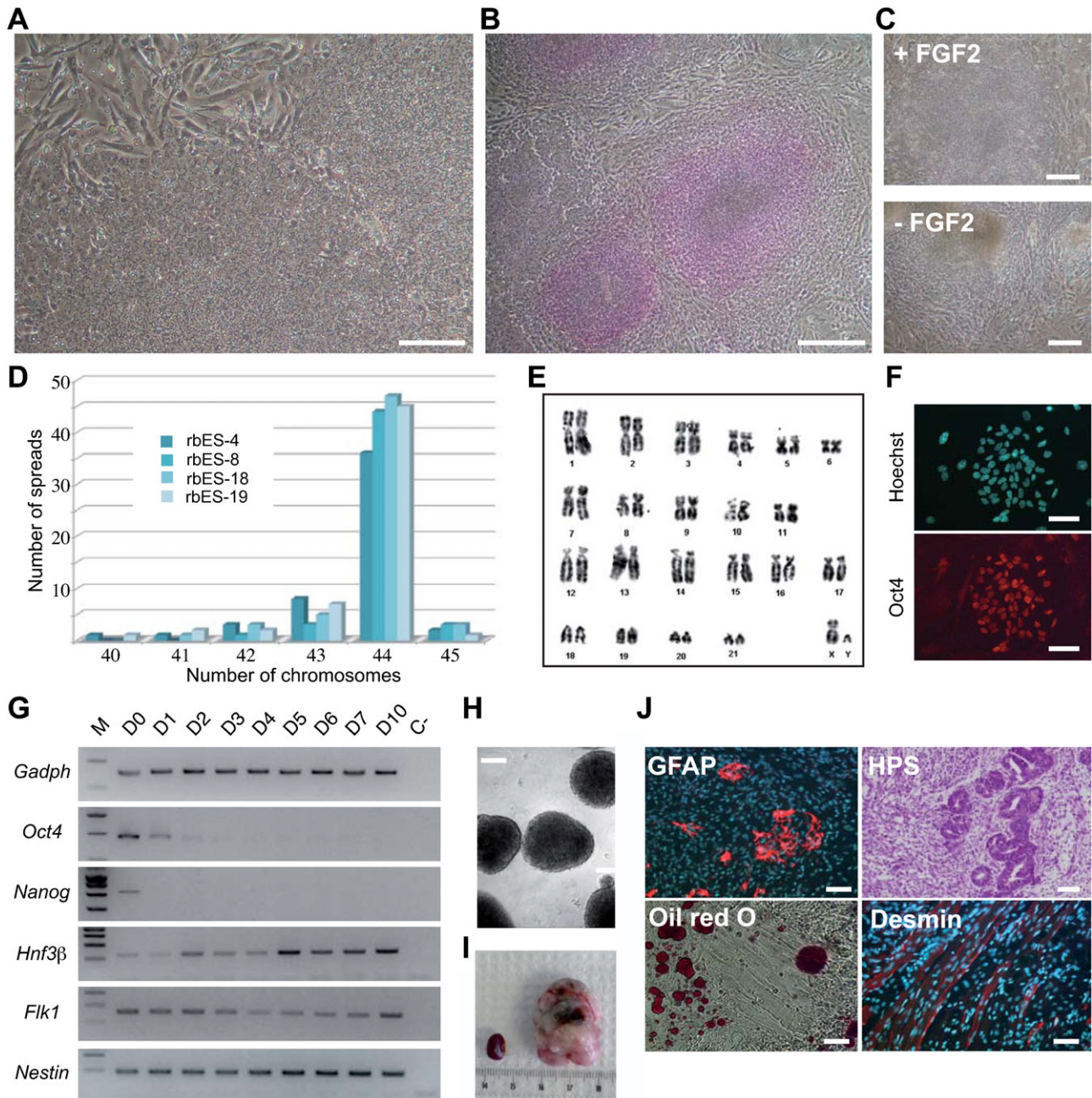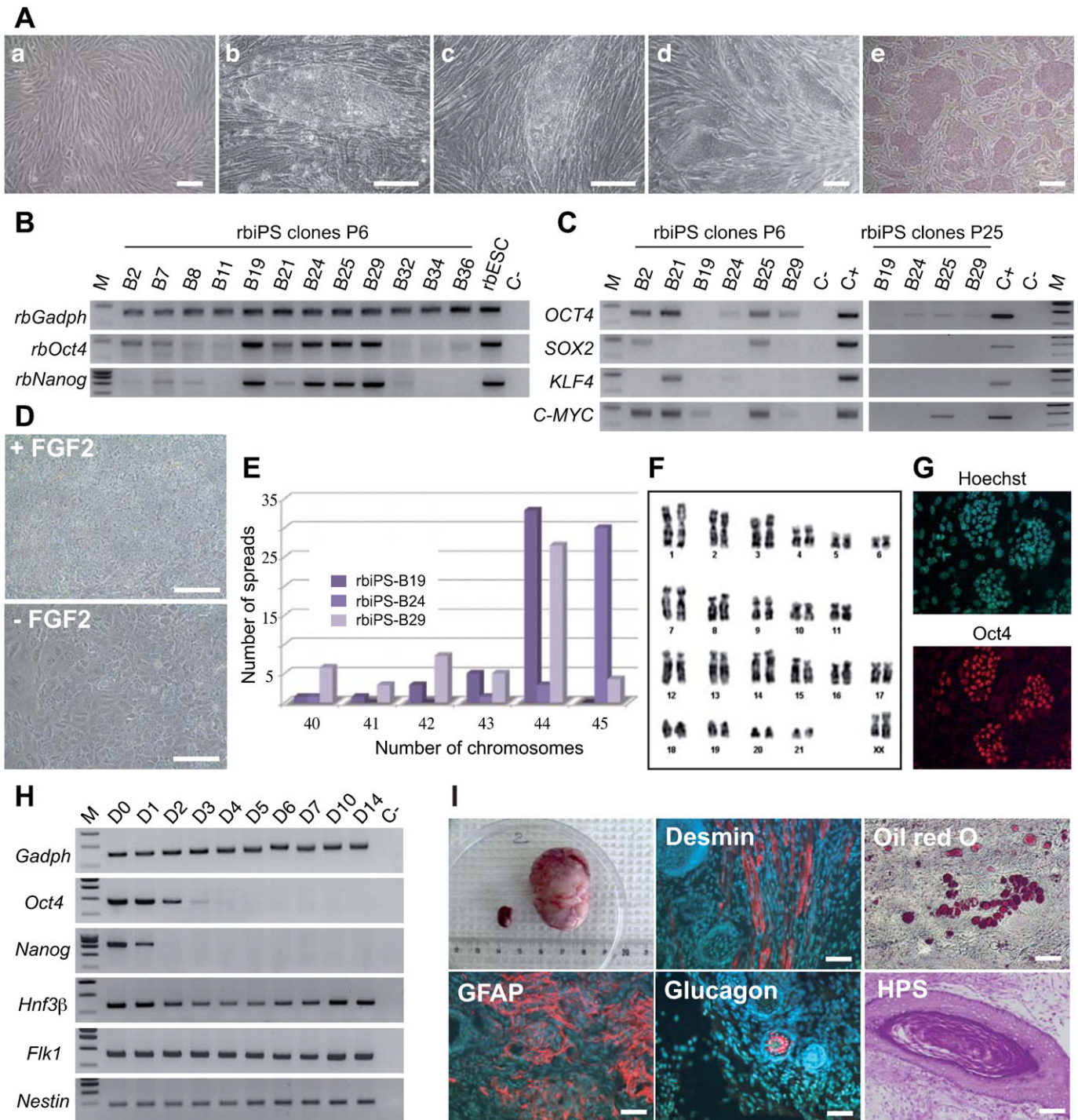
Fig. 1. Isolation and characterization of rbESC lines. (**A**) Phase-contrast image of rbES-18 cells at passage 28 (P28). (**B**) Alkaline phosphatase activity in rbES-18 cells. (**C**) Phase-contrast images of rbES-18 cells before and after FGF2 withdrawal for 24 h. (**D**) Histogram showing the distribution of chromosome numbers in rbES-4 at P13, rbES-8 at P17, rbES-18 at P15, and rbES-19 at P21. (**E**) G-banding karyotype of the rbES-18 line at P15. (**F**) Immunolabeling of rabbit Oct4. (**G**) RT-PCR analysis of pluripotency (*Nanog* and *Oct4*) and germ layer-specific (*Hnf3β*, *Flk1* and *Nestin*) gene expression during differentiation of rbES-18 cells induced by EB formation (days 0–10). (**H**) EB produced from rbES-18 cells. (**I**) Teratoma 31 days after injecting rbES-18 cells under the kidney capsule of SCID mice. (**J**) Histological section of the teratoma with tissue components of all 3 embryonic germ cell layers. Oil red O staining to detect adipocytes. Desmin and GFAP to detect muscle and glial cells, respectively. Gland structures could be identified after HPS staining. Scale bars: 50 μm.

the ESC *vs* iPSC status and not with the cell population heterogeneity observed as the SSEA expression.

Cell cycle characteristics demarcate the SSEA1⁺ rbiPS cells

PSCs show an unusual cell cycle structure that is characterized by a short G1 phase and a high proportion of cells in the S phase. In addition, they do not undergo cell-cycle arrest at the G1 checkpoint in response to DNA damage. Instead, they undergo growth arrest only at the G2 checkpoint (Aladjem et al., 1998; Fluckiger et al., 2006; Filipczyk et al., 2007). Therefore, we investigated whether rabbit PSCs displayed the same cell cycle characteristics. For the 4 rbESC lines, the G1, S, and G2/M phases were observed in $74\pm2.7\%$, $20\pm2.8\%$, and $6\pm2.9\%$ cell populations, respectively. For the 3 rbiPSC lines, the G1, S, and G2/

Fig. 2. **Generation and characterization of rbiPSC lines.** (**A**) Phase-contrast images of rbFs before (**a**) and after (**b–e**) infection with retroviral vectors expressing human transgenes; (b,c) primary colonies (P0) observed after 20 days of infection; (d) colonies observed at P6; (e) alkaline phosphatase activity at P6. (**B**) Expression of rabbit pluripotent genes *Oct4* and *Nanog* analyzed by RT-PCR in 12 independent rbiPSC clones at P6. (**C**) Expression of human transgenes analyzed by RT-PCR in 6 independent rbiPSC clones at P6 and P25. (**D**) Phase-contrast images of rbiPS-B19 cells before and after FGF2 withdrawal for 48 h. (**E**) Histogram showing the distribution of chromosome numbers in rbiPS-B19 at P37, rbiPS-B24 at P33, and rbiPS-B29 at P31. (**F**) G-banding karyotype of rbiPS-B19 line at P37. (**G**) Immunolabeling of rabbit Oct4. (**H**) RT-PCR analysis of pluripotency (*Nanog* and *Oct4*) and germ layer-specific (*Hnf3β*, *Flk1*, and *Nestin*) gene expression during differentiation of rbiPS-B19 cells induced by EB formation (days 0–14). (**I**) Teratoma at 30 days after injecting rbiPS-B19 cells under the kidney capsule of SCID mice, with tissue components of all the 3 embryonic germ cell layers. Histological section stained with HPS shows squamous epithelial cells. Oil red O staining to detect adipocytes. Desmin, GFAP, and glucagon to detect muscle, glial, and pancreatic α-cells, respectively. Scale bars: 50 μm.
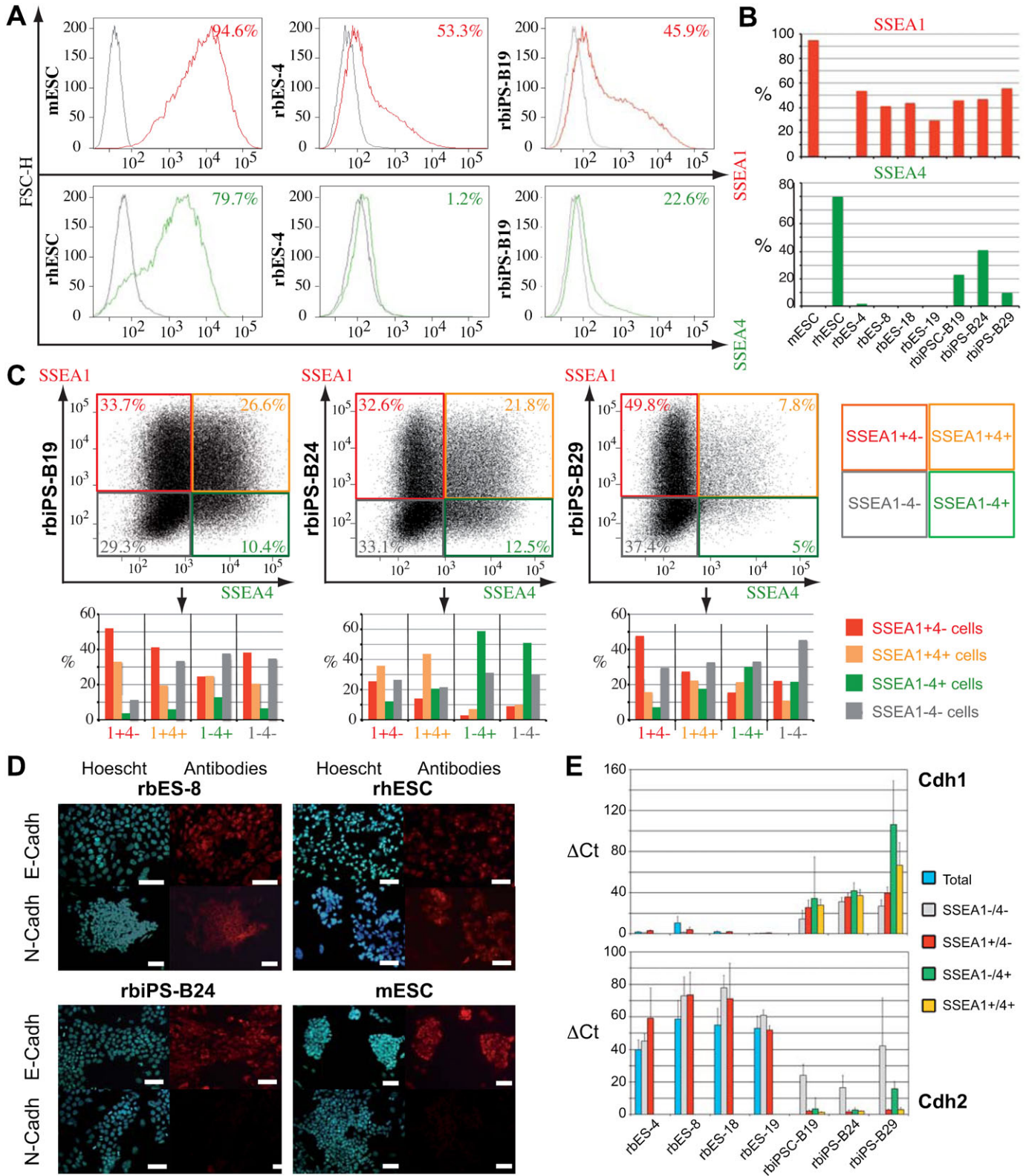
Fig. 3. **Expression of SSEA antigens and cadherins.** (**A**) Flow cytometry analysis of SSEA1 and SSEA4 marker expressions. (**B**) Histograms showing the percentages of SSEA1$^+$ and SSEA4$^+$ cells in various rbESC and rbiPSC lines. (**C**) Flow cytometry analysis of SSEA1 and SSEA4 marker expression in rbiPSC lines before and after FACS sorting of SSEA subpopulations. Upper panels: Dot plots of SSEA1- and SSEA4-associated fluorescence in rbiPS-B19, rbiPS-B24, and rbiPS-B29 lines before cell sorting. Bottom panels: Histograms showing the percentages of SSEA1$^+$/SSEA4$^-$ (1$^+$/4$^-$ cells), SSEA1$^+$/SSEA4$^+$(1$^+$/4$^+$ cells), SSEA1$^-$/SSEA4$^+$(1$^-$/4$^+$ cells), and SSEA1$^-$/SSEA4$^-$(1$^-$/4$^-$ cells) populations; these cell populations were derived from cultures of rbiPS lines after sorting each cell population, replating in FGF2-supplemented medium, and subsequent culture for 7 days. (**D**) Immunolabeling with antibodies for E- and N-cadherins. (**E**) Histograms showing mRNA levels (ΔCt) of the E-cadherin (*Cdh1*) and N-cadherin (*Cdh2*) as analyzed by qPCR for the entire cell population (total) and in various SSEA subpopulations, as indicated. mRNA levels were normalized to the mRNA level of *Tbp*. Scale bars: 50 μm.

M phases were observed in $43\pm2.4\%$, $38\pm3.5\%$, and $19\pm1.9\%$ cell populations, respectively (supplementary material Table S3). Thus, the percentage of rbPSCs in the S phase (20–38%) was higher than that in rbFs (7%) but lower than that in mESCs (68%), mEpiSCs (56%), and rhESCs (41%). The cell cycle distributions of the SSEA1$^+$ and SSEA4$^+$ subpopulations were also analyzed. Of all the analyzed cell lines, the SSEA1$^+$ subpopulations showed the lowest G1 and the highest S fractions than the SSEA1$^-$ and SSEA4$^+$ subpopulations. However, no SSEA1$^+$ subpopulation from any line analyzed showed a cell cycle distribution similar to that observed for SSEA1$^+$ mESCs (supplementary material Table S3).

To study the cell cycle response of rbPSCs to DNA damage, we analyzed the effects of doxorubicin, a DNA intercalator that induces double-strand breaks (Fig. 4). The G1 fraction of rbFs treated with doxorubicin for 24 h decreased from 80% to 41%, whereas the G2 fraction increased from 12% to 58%, indicating growth arrest in G1 and G2. In contrast, the G1 fraction of doxorubicin-treated mESCs decreased dramatically from 20% to 1%, whereas its G2 fraction increased from 11% to 99%, indicating a lack of G1 checkpoint in mouse PSCs and accumulation of cells at the G2 checkpoint. Similar results were obtained with rhESCs and mEpiSCs for which the G1 and S fractions virtually disappeared after doxorubicin treatment (Fig. 4A). The response of rbPSCs to doxorubicin treatment was more heterogeneous. They all showed moderate decreases in their G1 fractions (rbESCs, from 74% to 70%; rbiPSCs, from 43% to 20%) and significant increase in their G2 fractions (rbESCs, from 6% to 30%; rbiPSCs, from 19% to 80%). We assumed that this might be a reflection of the heterogeneity of rbPSC populations. Therefore, we analyzed the responses of different SSEA fractions to doxorubicin treatment. Only SSEA1$^+$/SSEA4$^-$ and SSEA1$^+$/SSEA4$^+$ subpopulations of rbiPSCs showed complete growth arrest in the G2 phase and did not show cell accumulation in the G1 phase; similar results were observed for mESCs, mEpiSCs, and rhESCs (Fig. 4A,B). All other fractions showed variable accumulation of cells in the G1 and G2 phases, as observed previously in the entire population. Of note, the SSEA1$^+$ subpopulation of rbESCs still showed accumulation in the G1 and G2 phases after doxorubicin treatment. Thus, these results indicate that only the SSEA1$^+$ subpopulation of rbiPSCs showed the cell cycle features of mESCs, mEpiSCs, and rhESCs (i.e. a shortened G1 phase, a high proportion of cells in the S phase, and absence of DNA damage checkpoint in G1). Neither the SSEA1$^+$ subpopulation of rbESCs nor the other subpopulations of rbiPSCs showed the cell cycle features of PSCs.

## Mouse Oct4 promoter activity and DNA methylation demarcates rbESC and rbiPSC lines

The distal element (DE) of Oct4 enhancer showed robust activity in ICM cells of mouse blastocyst, primordial germ cells, and mESCs. In contrast, it is minimally active in the epiblast of mouse postimplantation embryo and its EpiSC derivatives (Yeom et al., 1996; Tesar et al., 2007). Thus, DE activity can be used to discriminate between the naïve and primed states of pluripotency (Nichols and Smith, 2009). To evaluate the DE activity in rabbit preimplantation embryos, we used the L-SIN-EOS-C(3)-EiP lentiviral vector (designated EOS) that expressed GFP and the puromycin resistance gene under the transcriptional control of the minimal early transposon promoter and trimer of the CR4 enhancer (Hotta et al., 2009). The CR4 enhancer is a 146-bp fragment of the mouse DE element that recruits the Oct4, Sox2, and Sp1 transcription factors and recapitulates the regulation of the DE element in pluripotent and differentiated cell lines (Okumura-Nakanishi et al., 2005). A vector expressing GFP from the ubiquitous CAG promoter [GAE-CAG-eGFP/wpre, (Mangeot et al., 2002)] – designated GAE – was used as a control. Both lentiviral vectors were concentrated and injected under the zona pellucida of 8-cell-stage rabbit embryos. The embryos were then cultured to the mid-blastocyst stage before analysis with confocal microscopy. Fluorescent cells were observed in the trophoblast and ICM, with both control and EOS lentivectors, indicating the activity of the trimer of the CR4 enhancer in rabbit preimplantation embryos (Fig. 5A,B). DE activity in the trophoblast cells was consistent with previous observations, indicating that Oct4 was expressed in the trophoblast of the rabbit blastocyst (Kobolak et al., 2009).

To evaluate the DE activity in rabbit PSCs, rbESC, and rbiPSC lines were infected with EOS and GAE lentivectors and analyzed using flow cytometry after 4 days (Fig. 5C; supplementary material Fig. S4A). All cell lines infected with GAE showed green fluorescence ranging from 12% to 54% of positive cells according to the cell type (threshold set at 2.5×10^2). Approximately 60–95% of these GFP-positive cells showed fluorescence levels of $\geq10^3$. In contrast, fluorescence levels in EOS-infected cells varied dramatically between cell types. mESCs had the highest level (76% GFP-positive cells had fluorescence levels of $>10^3$). mEpiSCs showed no expression while rhESCs showed low expression (only 13% GFP-positive cells had fluorescence levels of $>10^3$). This indicates that rbESCs and iPSCs showed intermediate expression levels (rbES-4, 32%; rbES-8, 33%; rbES-19, 30%; rbiPS-B19, 42%; rbiPS-B24, 41%; and rbiPS-B29, 48%; Fig. 5C; supplementary material Fig. S4A). This suggested that the trimer of the CR4 enhancer was more active in rbPSCs than in mouse EpiSCs and primate ESCs.

The GFP expression level in EOS-infected cells was influenced by the infection rate. Therefore, to eliminate the confounding effect of the variations in infection rates between the cell lines, we calculated an expression index (I_E): $I_E = \dfrac{\%GFP^+_{\geq10^3}}{\%GFP^+_T}\times\%I_R$. $\%GFP^+\geq10^3$ is the percentage of GFP$^+$ cells with expression levels of $\geq10^3$; $\%GFP^+_T$ is the percentage of all GFP$^+$ cells; and I_R is the percentage of infected cells. Comparison of I_E values between cell lines showed that mESCs had the highest index, whereas rhESCs and EpiSCs had the lowest index. As determined from previous calculations, I_E of all rabbit lines was between that of mESCs and rhESCs, with all the 3 iPSCs lines showing higher I_E indices than the 3 ESC lines (Fig. 5D). From these experiments, we concluded that compared with rbESCs, rbiPSC lines could activate the mOct4 DE element at a higher level.

This conclusion was strongly reinforced by the results of puromycin selection of EOS-infected cells. All ESC and iPSC lines infected with EOS were cultured for 7 days in a medium supplemented with puromycin. Puromycin-resistant cells could be readily selected and expanded from mESCs and the 3 rbiPSC lines (designated rbiPS-B19-EOS, rbiPS-B24-EOS, and rbiPS-B29-EOS) (Fig. 5E). In contrast, no puromycin-resistant cells could be isolated from any of the rbESC lines infected with EOS lentivector. Therefore, we concluded that only iPSCs could
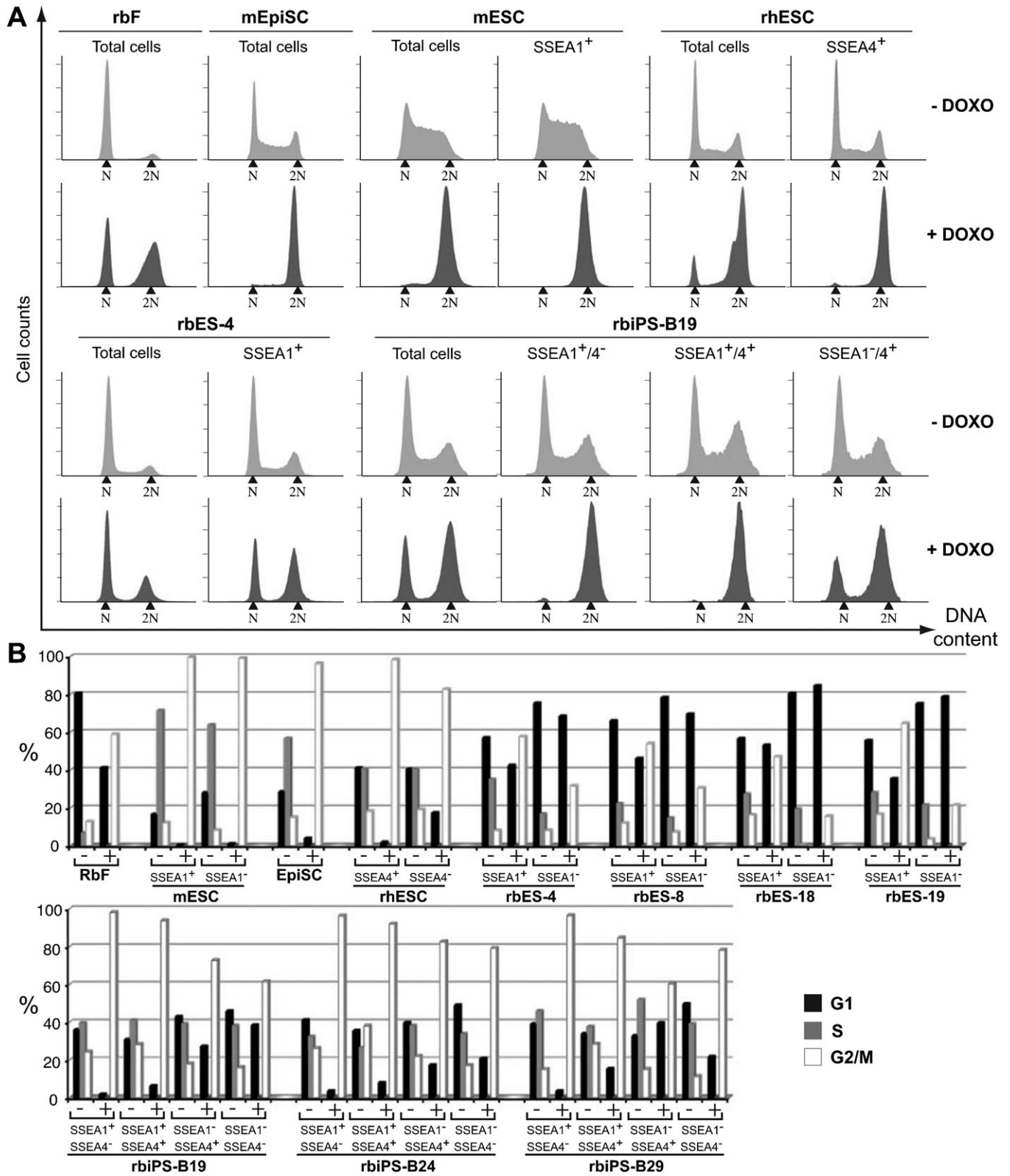
Fig. 4. Cell cycle analysis of rabbit PSCs. (A) Cell cycle profiles of rbFs, EpiSCs, mESCs, rhESCs, rbES-4, and rbiPS-B19 assessed using flow cytometry after staining with propidium iodide. Cell cycle distributions are shown for the total cell population and different SSEA subpopulations. + DOXO indicates treatment with 50 ng/ml doxorubicin for 24 h. (B) Histograms showing the percentage of cells in the G1, S, and G2/M phases of the cell cycle before and after doxorubicin treatment for different SSEA subpopulations. The percentages were calculated using ModFitLT.
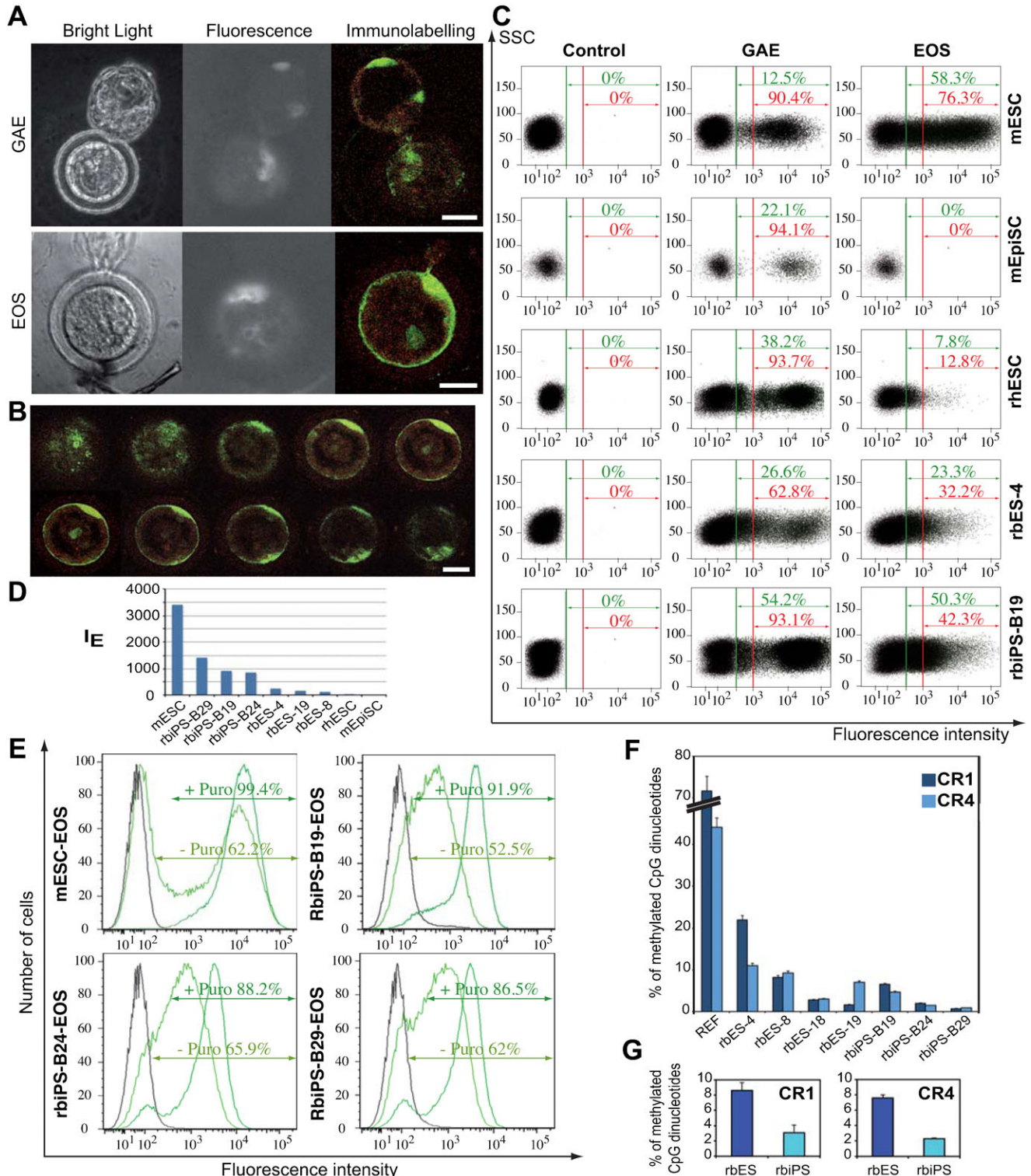
Fig. 5. Activity and methylation of mouse *Oct4* promoter in rabbit PSCs. (**A**) GFP immunolabeling of rabbit mid-stage blastocysts after injecting GAE and EOS lentivectors under the zona pellucida of 8-cell-stage embryos. (**B**) Serial confocal images of a blastocyst expressing EOS lentivector after GFP immunolabeling and costaining with propidium iodide. (**C**) Flow cytometry analysis of rbES-4, rbiPS-B19, mESCs, mEpiSCs, and rhESCs 4 days after infection with GAE and EOS lentivectors. For each dot plot, the numbers in green indicate the percentages of all GFP⁺ cells. Numbers in red indicate the percentages of GFP⁺ cells that had a fluorescence level of $\geqslant 10^3$ and which were normalized to the percentage of all GFP⁺ cells. (**D**) Histogram showing the results for GFP expression index: $I_E = \dfrac{\% GFP^{+}_{\geqslant 10^3}}{\% GFP^{+}_{T}} \times \% I_R$. (**E**) Flow cytometry analysis of mESC-EOS, rbiPS-B19-EOS, rbiPS-B24-EOS, and rbiPS-B29-EOS before ($-$ Puro) and after ($+$ Puro) selection with puromycin for 14 days. (**F**) Histogram showing the percentages of methylated CpG dinucleotides evaluated after bisulfite genomic sequencing of the *Oct4* promoter regions (CR1 and CR4) in all rabbit PSC lines and REFs. (**G**) Histogram comparing the percentages of methylated CpG dinucleotides between rbESCs and rbiPSCs in CR1 or CR4 region. Statistical analyses were conducted using analysis of variance followed by Fisher's test. Differences were considered significant for $P<0.01$. Scale bars: 50 μm.

activate the trimer of the CR4 enhancer at a level sufficient to confer resistance to puromycin. This conclusion was supported by the observation that the mean intensity of GFP fluorescence increased during puromycin selection of iPSCs infected with EOS, suggesting that only some rare cells expressing GFP at high levels were resistant to puromycin and expanded during selection. These puromycin-resistant cells had notably higher percentages of SSEA1$^+$ and SSEA4$^+$ cells than the original cells (i.e. before puromycin selection) (supplementary material Fig. S4B).

Regions CR1 and CR4 were chosen for the methylation study. Bisulfite genomic sequencing showed that both regions were 3–10 times more methylated in rabbit embryonic fibroblasts (REFs) than in rabbit PSCs (Fig. 5F; supplementary material Fig. S5). Regions CR1 and CR4 were less methylated in rbiPSCs than in rbESCs [CR1: 3.1% methylated CpG dinucleotides in rbiPSCs *vs* 8.6% in rbESCs ($P<0.01$); CR4: 2.3% methylated CpG dinucleotides in rbiPSCs *vs* 7.6% in rbESCs ($P<0.001$)] (Fig. 5G; supplementary material Fig. S5).

Gene expression profiling demarcates rbESC and rbiPSC lines

To further define the molecular properties of rbESCs and rbiPSCs, we purified the SSEA1$^+$/SSEA4$^-$, SSEA1$^+$/SSEA4$^+$, and SSEA1$^-$/SSEA4$^-$ subpopulations by FACS sorting in 4 rbESC lines and 2 rbiPSC lines and performed a global analysis of their expression profiles. For this, we used a rabbit-specific gene expression microarray containing approximately 13,000 independent genes. For each cell line (rbES-4, rbES-8, rbES-18, and rbES-19; rbiPS-B19 and rbiPS-B29) and SSEA subpopulations, 3 biological replicates were hybridized to the customized rabbit array. Hierarchical clustering of the normalized data showed that all subpopulations of rbESC lines were clustered on one side and all subpopulations of rbiPSC lines were clustered together on the other (Fig. 6A). This indicates that despite the heterogeneity observed in the cell lines, the variability is mainly associated with the cell status (rbESC *vs* rbiPSC) and not with the SSEA expression status.

To further examine the transcriptome of various rbESC and rbiPSC subpopulations, we examined the expression of rabbit homologs of 22 mouse genes [*Blimp1*, *Cdx2*, *Cdh1 (E-cadherin)*, *Cdh2 (N-cadherin)*, *Cldn6*, *Dax1 (NrOb1)*, *Dazl*, *Essrb*, *Fbxo15*, *Fgf4*, *Gbx2*, *Klf4*, *Lefty2*, *Nanog*, *Oct4 (Pou5f1)*, *Otx2*, *Pecam1*, *Pitx2*, *Piwil2*, *Rex1 (Zfp42)*, *Tbx3*, and *Tcfcp2l1*], the mRNA levels of which have been used to evaluate stemness and demarcate the naïve and primed pluripotent states in rodent cells (Tesar et al., 2007; Bao et al., 2009; Hanna et al., 2010; Tang et al., 2010; Wang et al., 2012). Of note, 12 genes (*Klf4*, *Cldn6*, *Otx2*, *Nanog*, *Oct4*, *Cdx2*, *Dazl*, *Rex1*, *Fbxo15*, *Pitx2*, *Tbx3*, and *Gbx2*) were represented on the microarray. The expression levels of these 22 genes were determined by qPCR for the SSEA1$^+$/SSEA4$^-$, SSEA1$^+$/SSEA4$^+$, SSEA1$^-$/SSEA4$^+$, and SSEA1$^-$/SSEA4$^-$ subpopulations purified from the 4 rbESC and 3 rbiPS lines (supplementary material Table S4; Fig. S6; Fig. 3E). In agreement with the microarray data, correlation clustering of the ΔCt values showed that the rbiPSC subpopulations showed fewer differences between them than with the rbESC subpopulations (Fig. 6B). To determine which genes accounted for the variations between rbESCs and rbiPSCs, PCA was performed from the qPCR data obtained with the SSEA1$^+$/SSEA4$^-$ and SSEA1$^+$/SSEA4$^+$ subpopulations (Fig. 6C). The first 2 principal components had 78% of the total variation. The first axis that

represented 56% of the total variability distinguished between rbESC and rbiPSC lines in accordance with correlation clustering analysis. The second axis represented 22% of the total variability and accounted for variability between cell lines. A graphical representation of gene dispersion in a trigonometric circle highlighted 2 clusters of genes: the first comprised *Cdh2*, *Gbx2*, and *Dax1* and the second comprised *Otx2*, *Pitx2*, *Cldn6*, *Cdh1*, *Essrb*, *Klf4*, *Dazl*, *Oct4*, *Piwil2*, *Nanog*, and *Pecam1* (Fig. 6D). Both clusters were clearly anticorrelated over the cell lines, indicating that their relative expression levels were mutually exclusive. Both clusters appeared to be representative because most of the distances between the origin and the projected variables were globally close to the maximum distance (i.e. 1). Thus, these 14 genes explained most of the variability observed between rbESCs and rbiPSCs (first axis in Fig. 6C). The other 8 genes (*Fgf4*, *Cdx2*, *Rex1*, *Tcfcp2l1*, *Lefty2*, *Fbxo15*, *Tbx3*, and *Blimp1*) mostly accounted for the variability observed between lines in each group (2nd axis Fig. 6D).

rbiPSCs are closer to ICM cells

We next examined which cell types (rbESCs *vs.* rbiPSCs) and which subpopulations (SSEA1$^+$ *vs.* SSEA4$^+$ *vs.* SSEA$^-$) showed the closest proximity to ICM cells of the rabbit embryo. To this end, the expression of the 22 genes was measured in the ICM of third-day rabbit mid-blastocysts (supplementary material Table S4) and compared to the expression measured in the rbESC and rbiPSC subpopulations. Calculation of the Euclidean distances between the ICM sample and each subpopulations showed that SSEA1$^+$ rbiPSCs were the closest to the ICM and the SSEA1$^-$ rbiPSCs were the farthest (Fig. 7A). Interestingly, all rbESC subpopulations, irrespective of their SSEA1 status, were more distantly related to the ICM than the SSEA1$^+$ rbiPSCs. The relative proximity of the SSEA1$^+$ rbiPSCs with the ICM could be further evidenced in a rank histogram of the relative expression level of the 22 genes (Fig. 7B,C). The RNA level of each gene in ICM cells were normalized to the mRNA level of *Tbp*, and the resultant ΔCt was ranked from the highest (*Oct4*: ΔCt=37.5) to the lowest (*Dax1*: ΔCt=0.0013). Most genes that were strongly expressed in rbiPSCs than in rbESCs (*Oct4*, *Cdh1*, *Essrb*, *Cldn6*, *Nanog*, *Klf4*, *Otx2*, *Dazl*, *Pitx2*, *Piwil2*, *Pecam1*; $P<0.05$) were highly expressed in the ICM (ΔCt>1). In contrast, genes that were strongly expressed in rbESCs (*Cdh2*, *Gbx2*, *Dax1*; $P<0.05$) were expressed at low levels in the ICM (ΔCt<0.1). Taken together, these results indicate that the gene expression profile of SSEA1$^+$ rbiPSCs best matched that of the ICM cells of rabbit preimplantation embryo.

Colonization of pre-implantation embryos by rbESCs and rbiPSCs

To evaluate the capacity of rbESCs to colonize pre-implantation embryos and contribute to the formation of ICM, 5–10 rbES-18 cells that expressed GFP were injected under the zona pellucida of 20 eight-cell-stage rabbit embryos. Of note rbES18 was derived from a GFP transgenic embryo (Al-Gubory and Houdebine, 2006) and GFP was expressed by all cells in this population (Fig. 8A). In a parallel experiment, rbES-18 SSEA1$^+$ cells were sorted by FACS and then injected into 67 eight-cell-stage embryos. All embryos were cultured until they reached the mid-blastocyst stage prior to GFP immunostaining and analysis by confocal microscopy (supplementary material Table S5; Fig. 8B). No GFP-expressing cells were observed in the 74
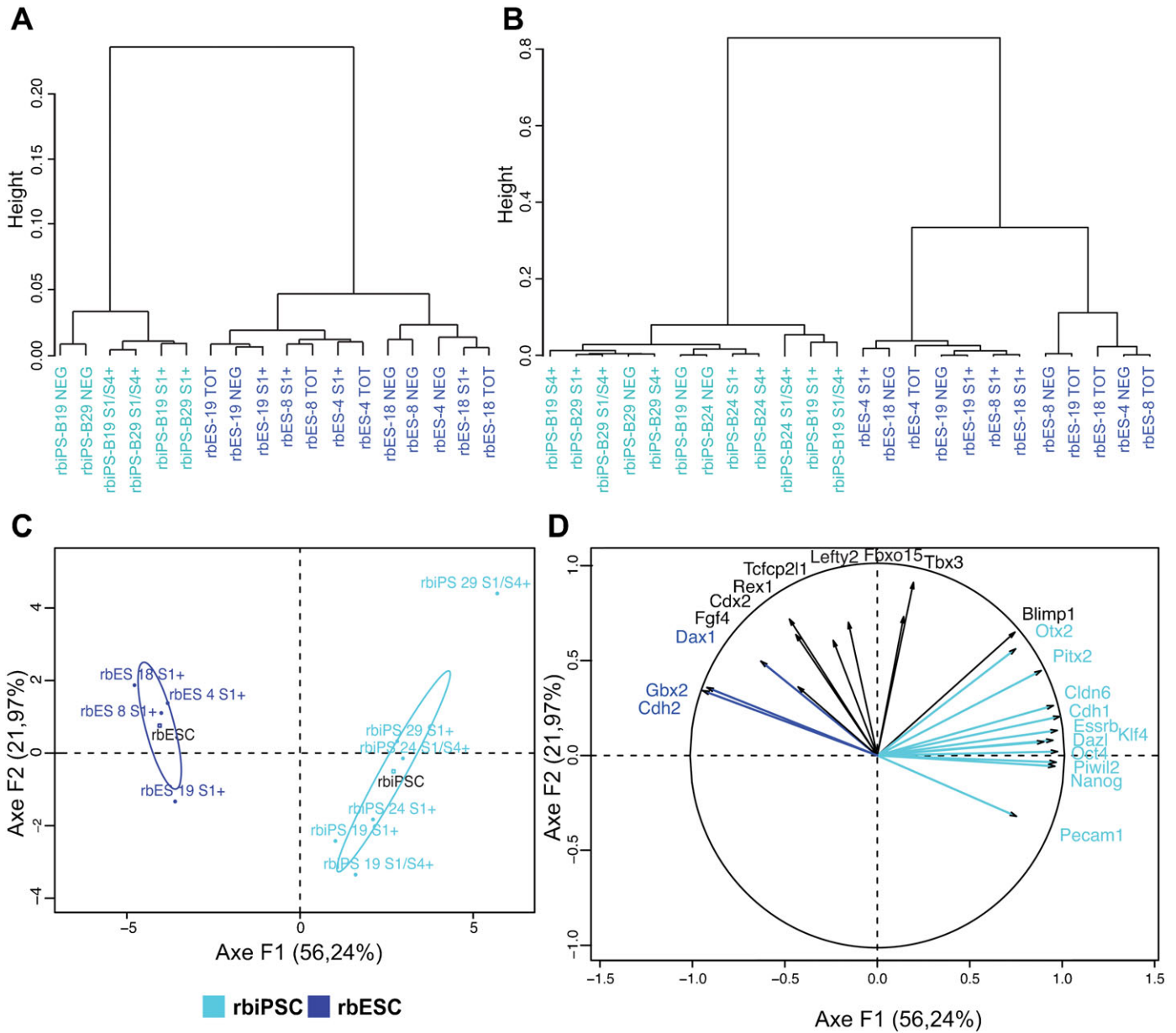
Fig. 6. Gene expression analysis for rbESCs and rbiPSCs. (A) Hierarchical clustering of transcriptome data (mean values/cell category) using Pearson correlation coefficient as a measure of distance between samples. (**B**) Correlation clustering for SSEA subpopulations of rbESCs and rbiPSCs (S1+: SSEA1+/SSEA4−; S4+: SSEA1−/SSEA4+; S1/S4+: SSEA1+/SSEA4+; NEG: SSEA1−/SSEA4−; TOT: total population) based on the RNA levels of the 22 genes (*Blimp1*, *Cdx2*, *Cdh1*, *Cdh2*, *Cldn6*, *Dax1*, *Dazl*, *Essrb*, *Fbxo15*, *Fgf4*, *Gbx2*, *Klf4*, *Lefty2*, *Nanog*, *Oct4*, *Otx2*, *Pecam1*, *Pitx2*, *Piwil2*, *Rex1*, *Tbx3*, and *Tcfcp2l1*) measured by qPCR. mRNA levels were measured in 3 biological replicates and 3 technical repeats, and normalized to *Tbp* expression levels. (**C**) Graphical representation of the first principal component of PCA for SSEA1+(S1+) and SSEA1+/SSEA4+(S1/S4+) subpopulations based on the RNA levels of the 22 genes that discriminated the 2 groups of relatively closer cell types. (**D**) Graphical representation of the first principal component of PCA for the 22 genes in a trigonometric circle that discriminated the 2 groups of anticorrelated genes (shown in dark blue and cyan).

embryos that had successfully developed to the blastocyst stage. In contrast, when 5–10 mES GFP+ cells (line CGR8-GFP) were injected into rabbit embryos at the same stage, all the resulting blastocysts (15) exhibited extensive colonization of ICM (Fig. 8C). Thus, rabbit early-cleavage-stage embryos were permissive to colonization by naïve mESCs but not by rbESCs.

We performed a similar experiment with rbiPS-B19 line. First, rbiPS-B19 cells were infected with the GAE lentivector that expressed GFP under the CAG promoter. GFP+ cells were sorted by FACS and then injected into 47 eight-cell-stage rabbit

embryos. All developed to the blastocyst stage, but only one embryo exhibited GFP+ cells in the ICM and in the trophoblast. Similarly, SSEA1+ rbiPS-B19-GFP cells were sorted prior to injection into 65 eight-cell-stage embryos. Only one blastocyst had GFP+ cells in the ICM after GFP immunostaining (Fig. 8D).

We thought that isolated rbiPSC survival would be very poor after injecting them into eight-cell-stage embryos and that this could explain the low rate of chimaeric blastocysts that was observed. To bypass the dissociation step, we generated aggregation chimaeras with 8-cell-stage embryos. Of note, this
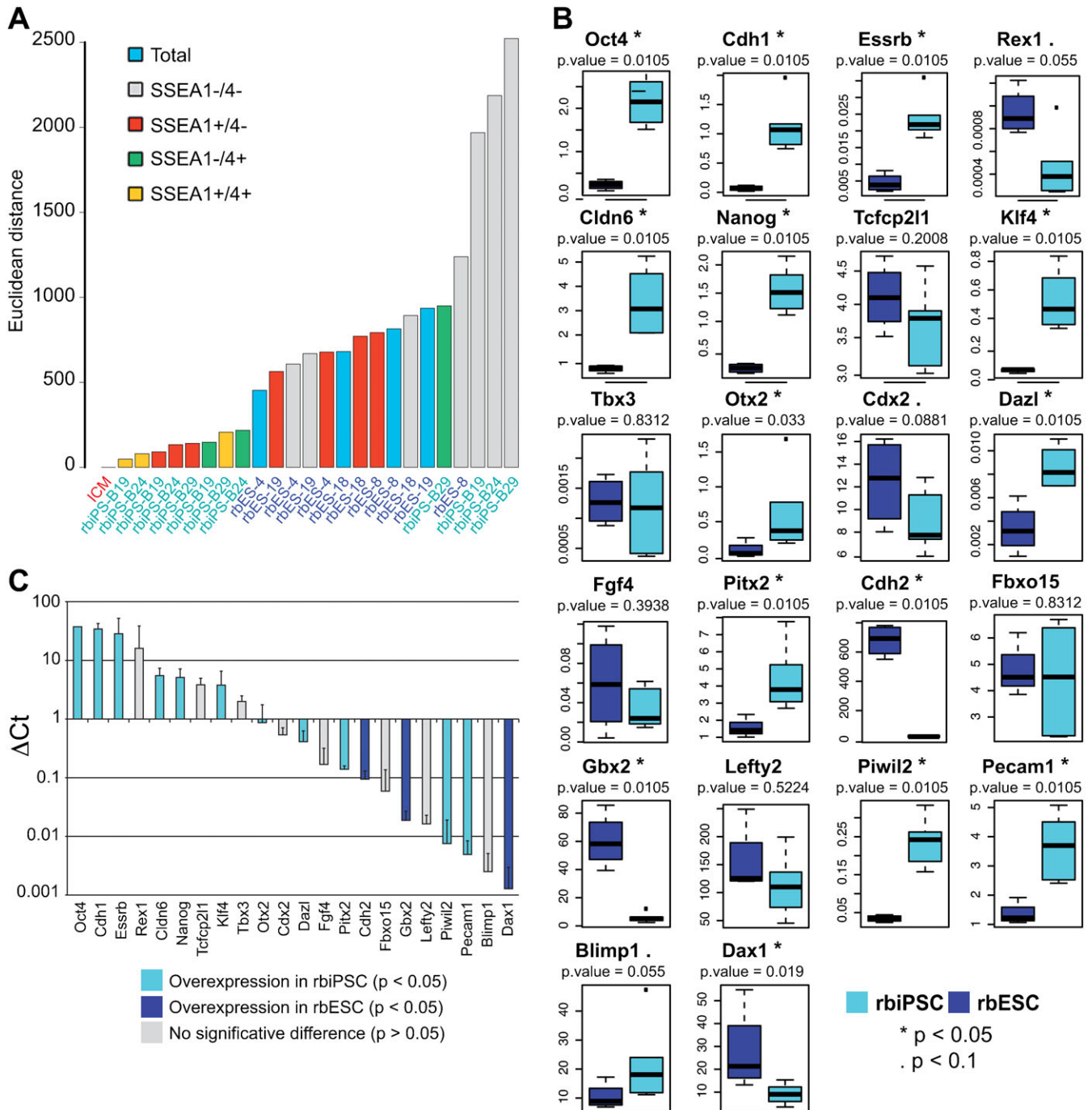
Fig. 7. Gene expression profiling in rbESCs and rbiPSC *vs.* ICM cells. (A) Histogram showing the Euclidean distances between the ICM cells and each subpopulations, as determined from the expression profiles of the 22 genes. Euclidean distances correspond to the value of a vectorial distance in a multidimensional orthonormal basis (the number of dimensions is the number of genes analyzed). An Euclidean distance D for a PSC subpopulation a was calculated using the following formula: $D = \sqrt{\left[(x_a - 1)^2 + (y_a - 1)^2 + \ldots + (n_a - 1)^2\right]}$ (1). x_a, y_a, and n_a represent the relative expression of each gene (x, y, and n) calculated by qPCR for the PSC subpopulation line a. (B) Histogram showing the ΔCt values calculated for each of the 22 genes in the SSEA1^{+} rbESCs (dark blue bars) and SSEA1^{+} rbiPSCs (cyan bars). (C) Histogram showing the ΔCt values calculated for each of the 22 genes in the rabbit ICM, normalized to the mRNA level of *Tbp* gene (ΔCt=1) and ranked from the highest (left) to the lowest (right). Cyan bars: genes highly expressed in rbiPSCs, as calculated in panel B; dark blue bars: genes highly expressed in rbESCs; grey bars: genes equally expressed in rbiPSCs and rbESCs.

technique requires removal of the mucous coat, which prevents embryo implantation into the uterus after transfer to surrogates (Murakami and Imai, 1996). For this goal, rbiPS-B19 cells were infected with ABP-RP-TLCLACZL, a lentiviral vector that expressed the lacZ gene under the control of the EF1α promoter. Viable β-galactosidase^{+} cells were isolated by iterative FACS sorting until a population of rbiPS-B19 cells that expressed β-galactosidase at a robust level could be stably expanded. The rbiPSC-B19-LacZ cells were subsequently infected with the EOS lentivector and selected with puromycin
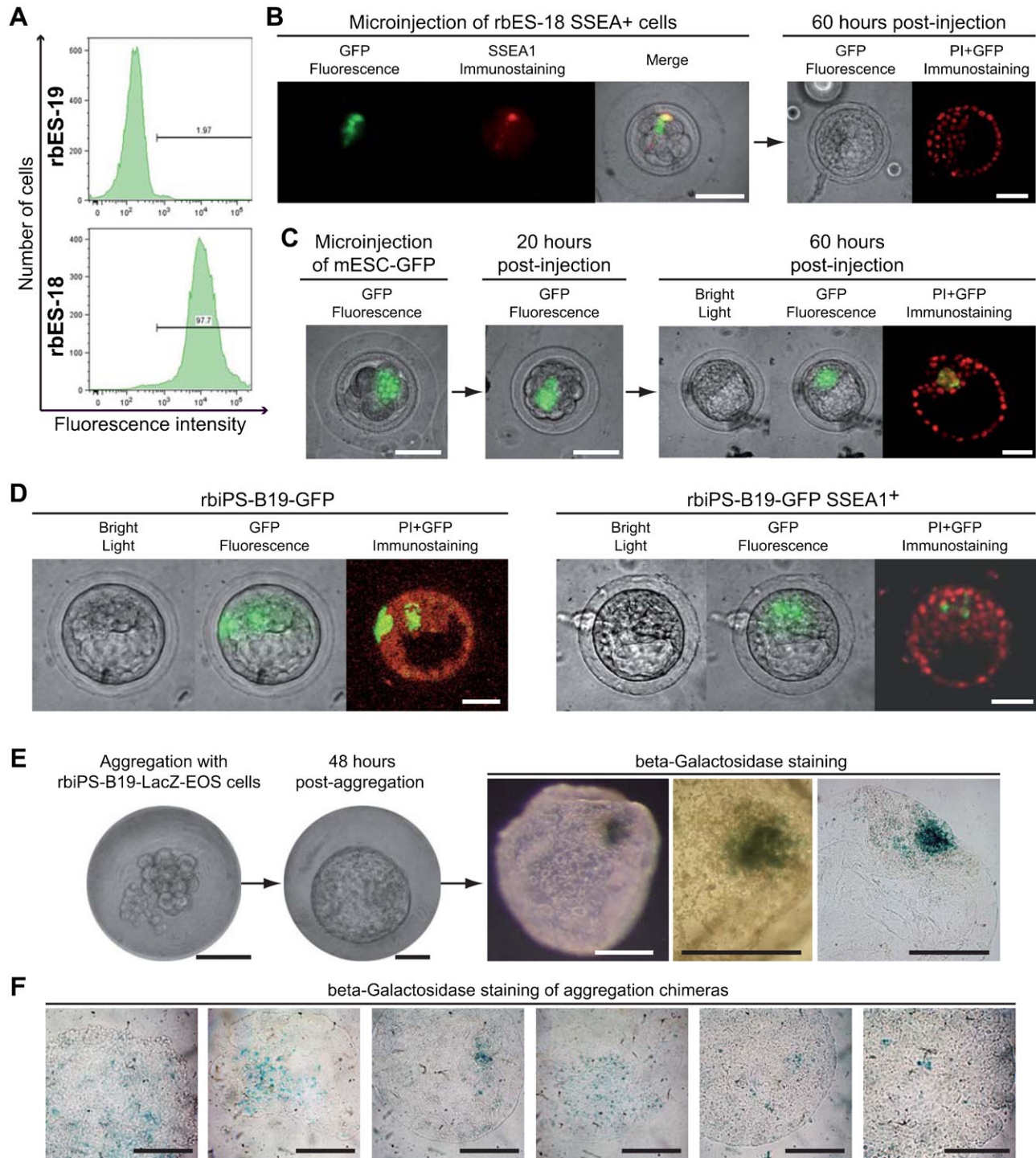
Fig. 8. Colonization of pre-implantation embryos. (**A**) Flow cytometry analysis of GFP expression in rbES-18 and rbES-19 cells derived from GFP-transgenic and non-transgenic blastocysts, respectively. (**B**) Microinjection of SSEA1^{+} rbES-18 cells into eight-cell-stage embryos and observation of developing embryos at the blastocyst stage. (**C**) Microinjection of mESCs (CGR8-GFP line) into rabbit eight-cell-stage embryos and observation of developing embryos at morula and blastocyst stages. (**D**) Observation of blastocyst-stage embryos resulting from the microinjection of rbiPS-B19-GFP and rbiPS-B19-GFP SSEA1^{+} cells into eight-cell-stage embryos. (**E**) Left panels: Phase-contrast images showing aggregation of an eight-cell-stage embryo with a clump of rbiPS-B19-LacZ-EOS cells, and the resulting blastocyst after *in vitro* culture for 48 hours. Right panels: β-galactosidase activity in the ICM of the blastocyst. (**F**) β-galactosidase activity in blastocysts resulting from aggregation of eight-cell-stage embryos with a clump of rbiPS-B19-LacZ-EOS cells and subsequent *in vitro* culture for 48 hours. Scale bars: 50 μm.

to generate a homogenous population of *mOct4* DE-positive cells (not shown). Clumps of 20–25 resulting rbiPSC-B19-LacZ-EOS cells were aggregated in the zona pellucida- and mucous

coat-free 8-cell-stage embryos and were subsequently cultured to the mid-blastocyst stage. We obtained 62 blastocysts, of which 10 had β-galactosidase^{+} cells in the ICM. In one case, the ICM

was heavily colonized by β-galactosidase^{+} cells (Fig. 8E,F; supplementary material Table S5).

Discussion

Using the molecular and functional criteria that characterize pluripotency in rodents and primates, we demonstrated that rbESCs and rbiPSCs show some key differences. First, similar to mECSs, rbiPSCs are resistant to trypsinization to single-cell suspensions, a procedure that induces extensive cell death and differentiation when applied to rbESCs, mouse EpiSCs (Tesar et al., 2007), and primate ESCs (Wianny et al., 2008). Second, similar to mESCs, rbiPSCs express elevated levels of E-cadherin, whereas rbESCs express both E- and N-cadherins similar to mouse EpiSCs and primate ESCs (Tesar et al., 2007; Hawkins et al., 2012). Third, the cell cycle of rbESCs had a longer G1 phase than the S and G2 phases and similar to somatic cells, they undergo growth arrest in the G1 phase after DNA damage. This is in sharp contrast to the SSEA1^{+} rbiPSCs as well as to all mouse and primate PSCs examined until date, which have a relatively short G1 phase and lack a DNA damage checkpoint in the G1 phase (Aladjem et al., 1998; Hong and Stambrook, 2004; Fluckiger et al., 2006; Filipczyk et al., 2007; Momcilovic et al., 2010). Fourth, the CR4 element of the mouse *Oct4* DE exhibits a more robust activity in rbiPSCs than in rbESCs. High CR4 element activity is observed in mESCs, whereas low activity is observed in mouse EpiSCs (Tesar et al., 2007). Fifth, the *Oct4* promoter is less methylated in the rbiPSCs than in the rbESCs. Sixth, rbESCs and rbiPSCs show distinct gene expression profiles. We identified 14 genes whose activity is different between rbiPSCs and rbESCs. Similar to that in mESCs, *Essrb*, *Klf4*, *Piwil2*, *Cdh1*, *Dazl*, and *Pecam1* are strongly expressed in rbiPSCs; however, they are expressed at low levels in rbESCs. Last, based on the expression of the 22 selected genes, rbiPSC lines are the closest to rabbit ICM, whereas the profiles of all rbESC lines are the farthest. Taken together, it can be concluded that rbiPSCs show many characteristic features of naïve pluripotency as defined in rodents, i.e. resistance to single-cell dissociation, no expression of N-cadherin, robust activity of the distal enhancer of mouse *Oct4*, and robust expression of ICM-specific markers. However, rbiPSCs do not show all the attributes of naïve pluripotency. For instance, they exploit FGF2 signaling for self-renewal, an attribute of primed pluripotency (Nichols and Smith, 2009). In addition, they do not express all the molecular markers of naïve pluripotency, including *Rex1*, *Tbx3*, *Gbx2*, *Fgf4*, and *Dax1* (Tesar et al., 2007). Furthermore, they show a reduced capacity to colonize the ICM after injection into rabbit blastocysts. Based on these observations, we propose that rbiPSCs self-renew in an intermediate state between naïve and primed pluripotency. Such an intermediate state may resemble the intermediate epiblast stem cells (IESCs) recently described in the mouse (Chang and Li, 2013). Like IESCs, rbiPSCs express *Rex1* (naïve pluripotency marker) and *Otx2* (primed pluripotency marker) at low levels, and express *Pecam1* (naïve pluripotency marker) and *Pitx2* (primed pluripotency marker) at high levels. Moreover, both rbiPSCs and IESCs can colonize the ICM after aggregation with morulas. In the case of IESCs, the IESC-derived ICM cells failed to contribute to post-implantation development. In the case of rbiPSCs, we could not address this question because the morula aggregation technique requires removal of the mucin coat, which prevents embryo implantation into the uterus after transfer to surrogates (Murakami and Imai, 1996).

However, the growth requirements of IESCs and rbiPSCs seem different. IESCs, which grow on gelatin, respond either to LIF or to activin to self-renew in the undifferentiate state. By contrast rbiPSCs grow on feeders and are strictly dependent on FGF2 signalling. Nevertheless, the possibility remains that rbiPSCs could also be dependent on LIF produced by feeder cells.

We have shown that rbESCs do not show all the attributes of pluripotent stem cells. In particular, they have a DNA damage checkpoint in the G1 phase like somatic cells. It is generally assumed that shortening the G1 phase sustains the pluripotent state by restricting the window of opportunity for differentiation cues (Mummery et al., 1987; Burdon et al., 2002; Sela et al., 2012; Coronado et al., 2013). In *bona fide* pluripotent stem cells, the lack of a DNA damage checkpoint in G1 might further reduce this window by preventing growth arrest at a critical point for self-renewal. Thus, rbESCs lack some key features of the pluripotent cell cycle, which might explain why they exhibit such a low proliferation rate and high spontaneous differentiation rate than rbiPSCs and primate ESCs.

To conclude, we have reported the first PSC lines in a non-rodent species that show characteristics of naïve pluripotency. These cells represent a first step towards genome engineering and production of germline chimeras in rabbits.

Materials and Methods
Rabbit breeding
Sexually mature New Zealand White rabbits were purchased from Hycole (Marcoing, France) or HyPharm (Roussay, France). Superovulations of females were induced as described previously (Salvetti et al., 2010). Sixty hours after artificial insemination, the fertilized embryos were flushed from explanted oviducts using Euroflush® (IMV Technologies) and cultured in TCM199 medium (Sigma) supplemented with 10% new-born calf serum (Sigma) at 38℃ in 5% CO_2.

Cell culture
Mouse embryonic fibroblasts (MEFs) were prepared from 12.5-day-old embryos from the OF1 strain (Charles River). Rabbit embryonic fibroblasts (REFs) were prepared from 12-day-old embryos from the New Zealand White (Hycole). Rabbit fibroblasts (rbFs) were prepared from the ear skin of a 5-month-old New Zealand White female. MEFs, REFs, rbFs, the 293T cell line (ATCC, CRL 11268), the rhesus monkey ESC (rhESC) line LyonES (Wianny et al., 2008), and mouse ESCs [mESCs, CGR8 line (Mountford et al., 1994)] were cultured as described elsewhere (Sandrin et al., 2002; Wianny et al., 2008; Savatier et al., 1996). EpiSCs were derived from epiblasts of 6.5-day-old mouse embryos of the OF1 strain and cultured as described previously (Brons et al., 2007). rbESCs and rbiPSCs were cultured on mitomycin C-treated MEFs (1.25×10^4 MEF/cm²) in DMEM/F12 medium supplemented with 20% knockout serum replacement, 1% non-essential amino acids and 1% of a solution of 10,000 U/ml penicillin + 10,000 U/ml streptomycin + 29.2 mg/ml L-glutamine, 1 mM sodium pyruvate and 100 μM 2-mercaptoethanol (Invitrogen). For rbESC and rbiPSCs culture, the medium was supplemented with 13 ng/ml or 10 ng/ml FGF2, respectively. rbiPSCs were routinely dissociated into single-cell suspensions after treatment with 0.05% trypsin–EDTA. rbESCs were dissociated into small clumps of cells after treatment with 1 mg/ml collagenase II (Sigma).

Immunosurgery
The mucin coat and the zona pellucida of rabbit blastocysts (70 to 72 h post-insemination; mid-blastocyst stage) were mechanically removed after brief exposure (2 min) to 5 mg/ml pronase (Sigma). ICMs were separated from the trophectoderm by immunosurgery after incubation of hatched blastocysts in anti-rabbit whole goat serum (Sigma) at 37℃ for 30 min and brief exposure (5 min) to guinea pig complement serum (Sigma). Isolated ICMs were transferred to four-well plates on mitomycin C-treated MEFs at a concentration of 3.5×10^4 cells/cm² in rbESC medium. After 5 to 6 days, the developing outgrowths were mechanically dissociated into small clumps and transferred onto fresh feeder cells at 2.5×10^4 cells/cm². All subsequent passages were performed by mechanical dissociation after treating colonies with collagenase II at 1 mg/ml, followed by plating cell clumps on feeder cells at a concentration of 1.25×10^4 cells/cm².

Virus production and cell infection
Plasmids used for producing retroviral and lentiviral vectors were either purchased from Addgene [pMXs-hOCT3/4 (17217), pMXs-hSOX2 (17218), pMXs-hKLF4

(17219), pMXs-hc-MYC (17220) (Takahashi et al., 2007) and pL-SIN-EOS-C(3+)-EiP (21313) (Hotta et al., 2009)] or obtained from Dr Cosset [pTG5349, phCMV-GP and pGAE-CAG-eGFP/wpre (Sandrin et al., 2002; Mangeot et al., 2002)] or Dr Suter [psPax2 and pMD2G (Suter et al., 2006)]. Virus production, concentration and titration were performed as previously described by transfection of 293T cells (Sandrin et al., 2002). Concentrated LacZ-expressing lentiviral particles were purchased from Allele Biotech (ABP-RP-TLCLACZL).

To generate rbiPSCs, 5×10^5 rbFs were infected twice at a two-day interval with 3×10^6 of viral particles, which contained equal parts of the four freshly produced hOct4, hSox2, hKlf4 and hMyc retroviruses [multiplicity of infection (m.o.i.)=8], in the presence of 4 µg/ml polybrene (Sigma). Three days after the second infection, rbFs were trypsinized into single cells and replated at low density (6×10^2 cells/cm^2) onto growth-inactivated MEFs in rbiPSC medium. The medium was changed every other day for 2 to 3 weeks until iPSC-like colonies appeared. To infect ESCs and iPSCs, the cells were plated on Matrigel (Beckton Dickinson) prior to infection with L-SIN-EOS-C(3+)-EiP and GAE-CAG-eGFP/wpre lentivectors at an m.o.i. of 5–10 in appropriate media supplemented with 6 µg/ml of polybrene. Rabbit eight-cell-stage embryos were infected by microinjection of 1 nl L-SIN-EOS-C(3+)-EiP and GAE-CAG-eGFP/wpre lentivectors (2×10^7 infectious particles/ml) under the mucous coat and zona pellucida.

Alkaline phosphatase and β-galactosidase detection, immunolabelling, flow cytometry and confocal microscopy analysis
Alkaline phosphatase and β-galactosidase activities were assessed using a PAL 86R-1KT kit (Sigma) and a GALS staining kit (Sigma), respectively, according to the manufacturer's instructions. To detect β-galactosidase activity in viable cells, LacZ-expressing cells were analysed by flow cytometry using a FluoReporter® lacZ flow cytometry kit (Molecular Probes) according to the manufacturer's instructions.

For immunolabelling, the cells were grown on cover slips pre-treated with gelatin and FBS and coated with feeder cells. The cells were fixed with 2% paraformaldehyde (PFA; Sigma) in phosphate-buffered saline (PBS) at 4℃ for 30 min, permeabilized in Tris-buffered saline (TBS, 50 mM Tris pH 7.6, 0.9% NaCl, 0.2% Triton X-100) and washed three times (10 min each) in TBS. Non-specific binding sites were blocked with TBS supplemented with 10% FBS and 1% bovine serum albumin (BSA) for 1 h and subsequently incubated overnight at 4℃ with primary antibodies (supplementary material Table S1). After three rinses (10 min each) with TBS, the cells were incubated with fluorochrome-conjugated secondary antibodies (supplementary material Table S1) at room temperature (RT) for 1 h, followed by DNA staining with 0.5 µg/ml Hoechst 33342 for 3 min. Cover slips were mounted with mounting medium M1289 (Sigma), fixed with DPX medium (Cell Path), examined under a conventional fluorescence microscope (Leica DMRE) and analysed with Mercator software (Exploranova). For flow cytometry analysis, the cells were immunolabelled using the same protocols and the same antibodies used for immunostaining on coverslips, except that incubation with antibodies was at RT for 30 min. The cells were analysed using a FACS Canto II cytometer and FACSDiva software (Becton Dickinson). The same protocol was used to detect GFP expression in rabbit blastocysts by immunolabelling, except that embryos were fixed with 2% PFA and permeabilized with 0.5% Triton X-100 in TBS. After DNA staining with 3 µg/ml of propidium iodide in 1% BSA, embryos were incubated sequentially in baths (30 min each) of 10%, 20% and 40% glycerol in TBS and then mounted on slides with mounting medium M1289 (Sigma) containing 0.1% p-phenylene-diamine (w/v) (Sigma). The embryos were observed by confocal microscopy (Leica TCS SP1 microscope with LSM software) at 488 nm and 555 nm (serial slices of 4 mm).

Real-time RT-PCR
Total RNA was isolated from cell clumps, cell pellets and embryoid bodies (EBs) using an RNeasy mini kit (Qiagen) according to the manufacturer's protocol and reverse-transcribed using 200 U of M-MLV retrotranscriptase (Promega) and random primer mix (MWG). Real-time PCR used the StepOnePlus real-time PCR system (Applied Biosystems) and Fast SBYR® Green Master Mix (Applied Biosystems) according to the manufacturer's instructions. Following 40 amplification cycles, melt-curve analysis was used to verify that only the desired PCR products had been amplified. PCR efficiency for both target and reference genes was determined from the relative quantitative values for calibrator-normalized target gene expression using StepOnePlus Software V2.1 (Applied Biosystems). In all cases, expression of the target genes was normalized to those of rabbit TATA-box binding protein (*Tbp*) gene. But the same results were obtained with a normalization with the mRNA level of rabbit *Gapdh* gene. All primers used for RT-PCR and qPCR are shown in supplementary material Table S2.

Karyotype analysis
Chromosome spreads were prepared according to standard procedures and stained with Giemsa solution (Sigma). Thirty to fifty metaphase spreads were counted for each of the rbESC and rbiPSC lines. For karyotyping, G-banding was performed using 0.045% trypsin in Ca^{2+}- and Mg^{2+}-free Tyrode (Sigma). For some rbESC

and rbiPSC line analysed, 4 to 20 banded karyotypes were evaluated for chromosomal rearrangements.

EB formation and teratoma production
For EB formation, rbESCs and rbiPSCs were dissociated into single cells using 0.05% trypsin, resuspended in rbESC medium without FGF2 and cultured in hanging drops. For teratoma formation, 2–5×10^6 rbESCs or rbiPSCs were injected under the kidney capsules of 8-week-old severe combined immunodeficient (SCID) mice (CB17/SCID, Charles River). After 4–7 weeks, the mice were euthanized and lesions were surgically removed and fixed in 10% neutral buffered formalin (Curtin Matheson Scientific, Inc.) for paraffin sections, or in 4% PFA for cryosections.

Cell cycle analysis
Cells were cultured for 24 h with 50 ng/ml of doxorubicin hydrochloride (Adriamycin®, Sigma). Single-cell suspensions were fixed with 70% ethanol at $-20℃$, rehydrated with PBS at 4℃ for 30 min, rinsed twice with PBS and incubated with 0.1 mg/ml of RNAse A at RT for 30 min. Propidium iodide (30 mg/ml) was added to the cells for 1 min before analysis with a FACS Canto II cytometer (Becton Dickinson). Data were acquired using FACSDiva software (Becton Dickinson). The percentages of G1-, S- and G2-phase cells were determined using ModFitLT software (Verity Software House).

DNA methylation analysis
The methylation profile of the rabbit Oct4 promoter (GenBank: AC235550.2) was determined by bisulfite mutagenesis and sequencing as previously described (Borghol et al., 2008). Two regions of the Oct4 promoter were subjected to duplex-nested PCR. Region 1 is situated between positions -307 and $+96$ (25 CpG), and encompasses Conserved Region 1 (CR1) as defined by Kobolak et al. (Kobolak et al., 2009). Region 2 is situated between positions -2060 and -1626 (17 CpG sites), and encompasses Conserved Region 4 (CR4). Sequence of primers specific for bisulfite-converted DNA are as follows: Region 1, external forward: 5′-GTTTTTTTAGGGAGGGGGTGAGAG-3′, external reverse: 5′-AAAACCTTAA-AAACTCAACCAAATCC-3′, internal forward: 5′-ATGGGGTGGAAGGGAT-TTTAG-3′, internal reverse: 5′-AAAATCCACCCAACCTAACTCC-3′; Region 2, external forward: 5′-GTTGGTTGGGTAGGAGTTTAT-3′, external reverse: 5′-TAACCCTATCAAACTTCTAAAAAACT-3′, internal forward: 5′-ATAAGTT-AAAGAGTTTTGTTTTTTGG-3′, internal reverse: 5′-AACTTCTAAAAAACT AAATAACCTAACTCT-3′. The PCR products were cloned into the pNZY28-A plasmid (Nzyteh; Portugal) and 24 PCR-positive colonies were sequenced for each PCR product (Biofidal, Lyon, France).

Rabbit microarray and hybridization
A customized rabbit microarray was designed starting from the commercially available Agilent rabbit microarray (G2519F), and including genes expressed during preimplantation development in the rabbit (B.S.-P., L.J. and V.D., unpublished data). Briefly, rabbit embryonic ESTs obtained from four suppressive subtractive cDNA hybridizations (SSH) were included in the custom-made microarray. ESTs expressed during the first cleavage stages, blastocyst stage, and early gastrulation embryos were sequenced (Léandri et al., 2009), assembled into contigs and annotated through homology searches against nucleic and proteic databases. Furthermore, candidate genes sourced from Ensembl Genome Browser (oryCun2.0), and associated with pluripotency or embryonic development, were added to the design. The best quality probes from the commercially available Agilent transcriptome-wide rabbit microarray was added, resulting in a microarray with 62, 976 probes including positive and negative controls. The 60-mer oligosequence probes were designed by eArray (https://earray.chem.agilent.com/earray), and were used for microarrays synthesis *in situ* using the Agilent SurePrint™ technology (Agilent Technologies, Mississauga, On, Canada) with a 8×60 K format. The custom microarray design of the platform has been submitted to the NCBI GEO (Gene Expression Omnibus). The accession number of the platform is GSE43403.

For hybridization, cyanine-3 (Cy3) labeled cRNAs were prepared from 0.2 µg RNA using the One-Color Microarray-Based Gene Expression Analysis Low Input Quick Amp Labeling kit (Agilent) according to the manufacturer's instructions. Dye incorporation and cRNA yield were checked with the NanoDrop ND-1000 Spectrophotometer. 0.6 µg of Cy3-labelled cRNA (specific activity >6.0 pmol Cy3/ug cRNA) was fragmented at 60℃ for 30 minutes following the manufacturer's instructions. Hybridizations were performed for 17 hours at 65℃ in a rotating Agilent hybridization oven. After hybridization, microarrays were washed 1 minute at room temperature with GE Wash Buffer 1 (Agilent) and 1 minute with 37℃ GE Wash buffer 2 (Agilent), then dried immediately. Slides were scanned immediately after washing on the Agilent DNA Microarray Scanner using one color scan setting for 8×60k array slides (Scan Area 61×21.6 mm). The scanned images were analyzed with Feature Extraction Software (Agilent, 7.10.3.1). Features flagged in Feature Extraction as Feature Non-uniform outliers were excluded. Normalization procedures were performed using R

statistical software (R: A language and environment for statistical computing (R Foundation for Statistical Computing), Vienna, Austria; 2012, R-Core-Team; http://www.r-project.org) and data were normalized using intra-array median substraction and log2 transformation.

Statistical analysis

Principal component analysis (PCA) was performed on qRT-PCR data (centered and reduced) using R statistical software (FactoMineR: Multivariate exploratory: data analysis and data mining with R; R package version 1.20, 2012, Husson et al.; http://cran.r-project.org/web/packages/FactoMineR/index.html). Other statistical analyses were done using the test of Kruskal–Wallis. Normalized transcriptome data were analyzed by hierarchical clustering using the Pearson correlation coefficient as a measure of distance.

Injection of cells into pre-implantation embryos and aggregation with morulas

For microinjection, ESCs and iPSCs were dissociated into single-cell suspensions. Five to 10 cells were microinjected under the mucous coat and zona pellucida of eight-cell-stage rabbit embryos. The embryos injected with GFP-expressing cells were cultured *in vitro* until they reached the mid-blastocyst stage, fixed in 2% PFA and immunostained with anti-GFP antibody.

For morula aggregation, fertilized eggs were harvested 20 hours after insemination, and cultured in RDH medium (Invitrogen), as described elsewhere (Jin et al., 2000). When they reached the eight-cell stage, embryos were treated with pronase to eliminate the zona pellucida and placed with clumps of 20–25 PSCs in microwells to induce aggregations, as described previously (Wood et al., 1993). Successful aggregates were cultured for 48 hours until they reached the blastocyst stage and subsequently analysed for β-galactosidase activity.

Competing Interests

The authors have no competing interests to declare.

References

Al-Gubory, K. H. and Houdebine, L. M. (2006). *In vivo* imaging of green fluorescent protein-expressing cells in transgenic animals using fibred confocal fluorescence microscopy. *Eur. J. Cell Biol.* **85**, 837-845.

Aladjem, M. I., Spike, B. T., Rodewald, L. W., Hope, T. J., Klemm, M., Jaenisch, R. and Wahl, G. M. (1998). ES cells do not activate p53-dependent stress responses and undergo p53-independent apoptosis in response to DNA damage. *Curr. Biol.* **8**, 145-155.

Bao, S., Tang, F., Li, X., Hayashi, K., Gillich, A., Lao, K. and Surani, M. A. (2009). Epigenetic reversion of post-implantation epiblast to pluripotent embryonic stem cells. *Nature* **461**, 1292-1295.

Borghol, N., Blachère, T. and Lefèvre, A. (2008). Transcriptional and epigenetic status of protamine 1 and 2 genes following round spermatids injection into mouse oocytes. *Genomics* **91**, 415-422.

Brons, I. G., Smithers, L. E., Trotter, M. W., Rugg-Gunn, P., Sun, B., Chuva de Sousa Lopes, S. M., Howlett, S. K., Clarkson, A., Ahrlund-Richter, L., Pedersen, R. A. et al. (2007). Derivation of pluripotent epiblast stem cells from mammalian embryos. *Nature* **448**, 191-195.

Burdon, T., Smith, A. and Savatier, P. (2002). Signalling, cell cycle and pluripotency in embryonic stem cells. *Trends Cell Biol.* **12**, 432-438.

Chang, K. H. and Li, M. (2013). Clonal isolation of an intermediate pluripotent stem cell state. *Stem Cells*.

Coronado, D., Godet, M., Bourillot, P. Y., Tapponnier, Y., Bernat, A., Petit, M., Afanassieff, M., Markossian, S., Malashicheva, A., Iacone, R. et al. (2013). A short G1 phase is an intrinsic determinant of naïve embryonic stem cell pluripotency. *Stem Cell Res.* **10**, 118-131.

Fang, Z. F., Gai, H., Huang, Y. Z., Li, S. G., Chen, X. J., Shi, J. J., Wu, L., Liu, A., Xu, P. and Sheng, H. Z. (2006). Rabbit embryonic stem cell lines derived from fertilized, parthenogenetic or somatic cell nuclear transfer embryos. *Exp. Cell Res.* **312**, 3669-3682.

Filipczyk, A. A., Laslett, A. L., Mummery, C. and Pera, M. F. (2007). Differentiation is coupled to changes in the cell cycle regulatory apparatus of human embryonic stem cells. *Stem Cell Res.* **1**, 45-60.

Fluckiger, A. C., Marcy, G., Marchand, M., Négre, D., Cosset, F. L., Mitalipov, S., Wolf, D., Savatier, P. and Dehay, C. (2006). Cell cycle features of primate embryonic stem cells. *Stem Cells* **24**, 547-556.

Hanna, J., Cheng, A. W., Saha, K., Kim, J., Lengner, C. J., Soldner, F., Cassady, J. P., Muffat, J., Carey, B. W. and Jaenisch, R. (2010). Human embryonic stem cells with biological and epigenetic characteristics similar to those of mouse ESCs. *Proc. Natl. Acad. Sci. USA* **107**, 9222-9227.

Hawkins, K., Mohamet, L., Ritson, S., Merry, C. L. and Ward, C. M. (2012). E-cadherin and, in its absence, N-cadherin promotes Nanog expression in mouse embryonic stem cells via STAT3 phosphorylation. *Stem Cells* **30**, 1842-1851.

Honda, A., Hirose, M., Inoue, K., Ogonuki, N., Miki, H., Shimozawa, N., Hatori, M., Shimizu, N., Murata, T., Hirose, M. et al. (2008). Stable embryonic stem cell lines in rabbits: potential small animal models for human research. *Reprod. Biomed. Online* **17**, 706-715.

Honda, A., Hirose, M. and Ogura, A. (2009). Basic FGF and Activin/Nodal but not LIF signaling sustain undifferentiated status of rabbit embryonic stem cells. *Exp. Cell Res.* **315**, 2033-2042.

Honda, A., Hirose, M., Hatori, M., Matoba, S., Miyoshi, H., Inoue, K. and Ogura, A. (2010). Generation of induced pluripotent stem cells in rabbits: potential experimental models for human regenerative medicine. *J. Biol. Chem.* **285**, 31362-31369.

Hong, Y. and Stambrook, P. J. (2004). Restoration of an absent G1 arrest and protection from apoptosis in embryonic stem cells after ionizing radiation. *Proc. Natl. Acad. Sci. USA* **101**, 14443-14448.

Hotta, A., Cheung, A. Y., Farra, N., Vijayaragavan, K., Séguin, C. A., Draper, J. S., Pasceri, P., Maksakova, I. A., Mager, D. L., Rossant, J. et al. (2009). Isolation of human iPS cells using EOS lentiviral vectors to select for pluripotency. *Nat. Methods* **6**, 370-376.

Jin, D. I., Kim, D. K., Im, K. S. and Choi, W. S. (2000). Successful pregnancy after transfer of rabbit blastocysts grown *in vitro* from single-cell zygotes. *Theriogenology* **54**, 1109-1116.

Kobolak, J., Kiss, K., Polgar, Z., Mamo, S., Rogel-Gaillard, C., Tancos, Z., Bock, I., Baji, A. G., Tar, K., Pirity, M. K. et al. (2009). Promoter analysis of the rabbit POU5F1 gene and its expression in preimplantation stage embryos. *BMC Mol. Biol.* **10**, 88.

Léandri, R. D., Archilla, C., Bui, L. C., Peynot, N., Liu, Z., Cabau, C., Chastellier, A., Renard, J. P. and Duranthon, V. (2009). Revealing the dynamics of gene expression during embryonic genome activation and first differentiation in the rabbit embryo with a dedicated array screening. *Physiol. Genomics* **36**, 98-113.

Mangeot, P. E., Duperrier, K., Nègre, D., Boson, B., Rigal, D., Cosset, F. L. and Darlix, J. L. (2002). High levels of transduction of human dendritic cells with optimized SIV vectors. *Mol. Ther.* **5**, 283-290.

Momcilovic, O., Knobloch, L., Fornsaglio, J., Varum, S., Easley, C. and Schatten, G. (2010). DNA damage responses in human induced pluripotent stem cells and embryonic stem cells. *PLoS ONE* **5**, e13410.

Mountford, P., Zevnik, B., Düwel, A., Nichols, J., Li, M., Dani, C., Robertson, M., Chambers, I. and Smith, A. (1994). Dicistronic targeting constructs: reporters and modifiers of mammalian gene expression. *Proc. Natl. Acad. Sci. USA* **91**, 4303-4307.

Mummery, C. L., van den Brink, C. E. and de Laat, S. W. (1987). Commitment to differentiation induced by retinoic acid in P19 embryonal carcinoma cells is cell cycle dependent. *Dev. Biol.* **121**, 10-19.

Murakami, H. and Imai, H. (1996). Successful implantation of *in vitro* cultured rabbit embryos after uterine transfer: a role for mucin. *Mol. Reprod. Dev.* **43**, 167-170.

Nichols, J. and Smith, A. (2009). Naive and primed pluripotent states. *Cell Stem Cell* **4**, 487-492.

Okumura-Nakanishi, S., Saito, M., Niwa, H. and Ishikawa, F. (2005). Oct-3/4 and Sox2 regulate Oct-3/4 gene in embryonic stem cells. *J. Biol. Chem.* **280**, 5307-5317.

Salvetti, P., Buff, S., Afanassieff, M., Daniel, N., Guérin, P. and Joly, T. (2010). Structural, metabolic and developmental evaluation of ovulated rabbit oocytes before and after cryopreservation by vitrification and slow freezing. *Theriogenology* **74**, 847-855.

Sandrin, V., Boson, B., Salmon, P., Gay, W., Nègre, D., Le Grand, R., Trono, D. and Cosset, F. L. (2002). Lentiviral vectors pseudotyped with a modified RD114 envelope glycoprotein show increased stability in sera and augmented transduction of primary lymphocytes and CD34+ cells derived from human and nonhuman primates. *Blood* **100**, 823-832.

Savatier, P., Lapillonne, H., van Grunsven, L. A., Rudkin, B. B. and Samarut, J. (1996). Withdrawal of differentiation inhibitory activity/leukemia inhibitory factor

up-regulates D-type cyclins and cyclin-dependent kinase inhibitors in mouse embryonic stem cells. *Oncogene* **12**, 309-322.

Sela, Y., Molotski, N., Golan, S., Itskovitz-Eldor, J. and Soen, Y. (2012). Human embryonic stem cells exhibit increased propensity to differentiate during the G1 phase prior to phosphorylation of retinoblastoma protein. *Stem Cells* **30**, 1097-1108.

Suter, D. M., Cartier, L., Bettiol, E., Tirefort, D., Jaconi, M. E., Dubois-Dauphin, M. and Krause, K. H. (2006). Rapid generation of stable transgenic embryonic stem cell lines using modular lentivectors. *Stem Cells* **24**, 615-623.

Takahashi, K., Tanabe, K., Ohnuki, M., Narita, M., Ichisaka, T., Tomoda, K. and Yamanaka, S. (2007). Induction of pluripotent stem cells from adult human fibroblasts by defined factors. *Cell* **131**, 861-872.

Tang, F., Barbacioru, C., Bao, S., Lee, C., Nordman, E., Wang, X., Lao, K. and Surani, M. A. (2010). Tracing the derivation of embryonic stem cells from the inner cell mass by single-cell RNA-Seq analysis. *Cell Stem Cell* **6**, 468-478.

Tesar, P. J., Chenoweth, J. G., Brook, F. A., Davies, T. J., Evans, E. P., Mack, D. L., Gardner, R. L. and McKay, R. D. (2007). New cell lines from mouse epiblast share defining features with human embryonic stem cells. *Nature* **448**, 196-199.

Wang, S., Tang, X., Niu, Y., Chen, H., Li, B., Li, T., Zhang, X., Hu, Z., Zhou, Q. and Ji, W. (2007). Generation and characterization of rabbit embryonic stem cells. *Stem Cells* **25**, 481-489.

Wang, S., Shen, Y., Yuan, X., Chen, K., Guo, X., Chen, Y., Niu, Y., Li, J., Xu, R. H., Yan, X. et al. (2008). Dissecting signaling pathways that govern self-renewal of rabbit embryonic stem cells. *J. Biol. Chem.* **283**, 35929-35940.

Wang, L., Xue, Y., Shen, Y., Li, W., Cheng, Y., Yan, X., Shi, W., Wang, J., Gong, Z., Yang, G. et al. (2012). Claudin 6: a novel surface marker for characterizing mouse pluripotent stem cells. *Cell Res.* **22**, 1082-1085.

Wianny, F., Bernat, A., Huissoud, C., Marcy, G., Markossian, S., Cortay, V., Giroud, P., Leviel, V., Kennedy, H., Savatier, P. et al. (2008). Derivation and cloning of a novel rhesus embryonic stem cell line stably expressing tau-green fluorescent protein. *Stem Cells* **26**, 1444-1453.

Wood, S. A., Allen, N. D., Rossant, J., Auerbach, A. and Nagy, A. (1993). Non-injection methods for the production of embryonic stem cell-embryo chimaeras. *Nature* **365**, 87-89.

Yeom, Y. I., Fuhrmann, G., Ovitt, C. E., Brehm, A., Ohbo, K., Gross, M., Hübner, K. and Schöler, H. R. (1996). Germline regulatory element of Oct-4 specific for the totipotent cycle of embryonal cells. *Development* **122**, 881-894.